Inorganic Chemistry

Article

pubs.acs.org/IC

Toward Equatorial Planarity about Uranyl: Synthesis and Structure of Tridentate Nitrogen-Donor $\{UO_2\}^{2+}$ Complexes

Roy Copping,*[,†,▽] Byoungseon Jeon,[‡,§,○] C. Das Pemmaraju,[†,∥] Shuao Wang,[†] Simon J. Teat,[⊥] Markus Janousch,[†,#] Tolek Tyliszczak,[⊥] Andrew Canning,*[,‡,§] Niels Grønbech-Jensen,[‡,§] David Prendergast,*[,∥] and David K. Shuh*[,†]

[†]Chemical Sciences Division, The Glenn T. Seaborg Center, Lawrence Berkeley National Laboratory, Berkeley, California 94720, United States

[‡]Department of Applied Science, University of California, Davis, California 95616 United States

[§]Computational Research Division, Lawrence Berkeley National Laboratory, Berkeley California 94720, United States

[∥]The Molecular Foundry, Materials Sciences Division, Lawrence Berkeley National Laboratory, Berkeley, California 94720, United States

[⊥]Advanced Light Source, Lawrence Berkeley National Laboratory, Berkeley, California 94720, United States

[#]Laboratory for Synchrotron Radiation, Paul Scherrer Institute, Villigen, 5232 Switzerland

Supporting Information

ABSTRACT: The reaction of $UO_2Cl_2{\cdot}3THF$ with the tridentate nitrogen donor ligand 2,6-bis(2-benzimidazolyl)pyridine (H_2BBP) in pyridine leads to the formation of three different complexes: $[(UO_2)(H_2BBP)Cl_2]$ (**1**), $[(UO)_2(HBBP)(Py)Cl]$ (**2**), and $[(UO_2)(BBP)(Py)_2]$ (**3**) after successive deprotonation of H_2BBP with a strong base. Crystallographic determination of **1**−**3** reveals that increased charge through ligand deprotonation and displacement of chloride leads to equatorial planarity about uranyl as well as a more compact overall coordination geometry. Near-Edge X-ray Absorption Fine Structure (NEXAFS) spectra of **1**−**3** at the U-4d edges have been recorded using a soft X-ray Scanning Transmission X-ray Microscope (STXM) and reveal the uranium $4d_{5/2}$ and $4d_{3/2}$ transitions at energies associated with uranium in the hexavalent oxidation state. First-principles Density Functional Theory (DFT) electronic structure calculations for the complexes have been performed to determine and validate the coordination characteristics, which correspond well to the experimental results.

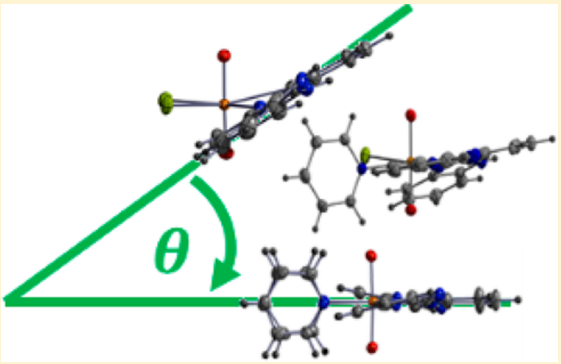

INTRODUCTION

The discovery of suitable starting materials for access into uranyl(VI), $\{UO_2\}^{2+}$, chemistry under anhydrous conditions has enabled the field of nonaqueous uranium coordination chemistry to flourish over the past two decades.[1−4] Expansion into anaerobic and anhydrous conditions has motivated the use of multidentate ligands containing nitrogen functional groups as well as weakly coordinating, polarizable ligands referred to as soft ligands, in addition to the more conventional hard-donor (e.g., oxygen and chlorine) systems predominantly studied in aqueous media.[5−7] Employing the redox stable and sterically demanding linear uranyl, $\{O{=}U{=}O\}^{2+}$, cation in a diverse range of ligand systems is providing an enhanced understanding of the structural, electronic, and chemical aspects of the uranyl cation. In turn, new chemistry with $\{UO_2\}^{2+}$ is promoting the development of new principles and theories of a moiety once believed to be fully understood.[8] Uranyl chemistry outside of aqueous conditions is continuing to broaden and expand, attracting great interest and producing new and exciting results with a recent focus on lower valent uranyl(V) chemistry and functionalization of the uranyl(VI) oxo ligand.[9−14] In multidentate donor ligand systems, the chemistry of $\{UO_2\}^{2+}$ has shown tremendous diversity in recent years with ligands adopting strained coordination geometries about uranyl to satisfy the equatorial coordination sphere.[14−22] The traditional pentagonal bipyramidal coordination sphere about uranium has shown tremendous deviation from ideal geometries in such complexes with severe distortions from linearity and lengthening of the axial $\{O{=}U{=}O\}^{2+}$ reported. It has also been suggested that out of plane bonding by equatorial ligands could be more prevalent for N-donor ligands.[10,20] Complexation with electron rich ligands in the equatorial plane can ultimately increase the Lewis basicity of the axial oxygens, which in turn can coordinate to a Lewis acid.[18,23] The innovative uranium complexes are providing new insights into nonaqueous

Received: October 19, 2013
Published: February 14, 2014

   dx.doi.org/10.1021/ic4026359 | Inorg. Chem. 2014, 53, 2506−2515

uranyl(VI) coordination chemistry and challenging long-held concepts about the chemistry of $\{UO_2\}^{2+}$ while increasing the knowledge of reactivity, bonding, and structure within uranyl complexes. Exploration of novel uranyl complexes is important for understanding the seminal role of the $\{UO_2\}^{2+}$ structural unit in actinide science that includes current and future nuclear fuel cycles, environmental remediation, safe storage of nuclear materials, and the long-term immobilization of nuclear waste.

The electronically tunable nitrogen-donor ligand 2,6-bis(2-benzimidazolyl)pyridine (BBP), which can be functionalized at the imidazole positions, has been studied as a sensitizer for lanthanide luminescence and has also shown potential as a low valent actinide sequestering agent.[24−30] In this instance, the free base derivative of 2,6-bis(2-benzimidazolyl)pyridine (H_2BBP) has been employed and successively deprotonated with sodium hydride to produce new mono- (NaHBBP) and disodium (Na_2BBP) substituted salts, and the reactivity of these species has been explored with uranyl(VI) chloride. This systematic approach to synthesizing N-donor uranyl complexes has provided a system with discrete chemical, structural, and electronic (bonding) properties within a N-donor uranyl system and a preliminary probe of the uranium 4d edges by scanning transmission X-ray microscopy is described. The synthesis and structural characterization of three new $\{UO_2\}^{2+}$ tridentate N-donor complexes **1**−**3** is reported herein. In addition, first-principles DFT-based calculations have been employed to compare coordination environments and electronic structures of **1**−**3** to investigate the origin of the geometrical differences found in these uranyl complexes.

EXPERIMENTAL SECTION

Syntheses Caution! *^{238}U is a low specific-activity α-particle emitting radionuclide, and its use presents hazards to human health. This research was conducted in a radiological facility with appropriate analyses of these hazards and implementation of controls for the safe handling and manipulation of toxic and radioactive materials.*

All experiments were performed in a MBraun Labmaster 100 argon atmosphere glovebox, except for the preparation of BBP·xH_2O, which was performed in a fume hood. All solvents were purchased either anhydrously from a reputable supplier and/or distilled over an appropriate desiccant, degassed, stored over a mixture of 4 Å/13X molecular sieves, and tested with a solution of sodium benzophenone prior to use. Chemicals were purchased from Aldrich; $UO_2Cl_2(THF)_3$ was prepared according to literature procedures.[4] ^1H and ^{13}C NMR were recorded on a Bruker Advance 300 MHz spectrometer and referenced to residual proton and carbon solvent resonances. Elemental analyses were performed by the Micro-Mass facility in the Department of Chemistry at the University of California at Berkeley. Infrared spectra were recorded with a Mattson Sirius 100 spectrometer.

Synthesis of 2,6-Bis(2-benzimidazolyl)pyridine·H_2O [H_2BBP·xH_2O]. 2,6-Bis(2-benzimidazyl)pyridine was synthesized by modification of a previously reported method.[31] *o*-Phenylenediamine (4.33 g, 40 mmol) and 2,6-dicarboxylic acid pyridine (3.35 g, 20 mmol) were heated in an autoclave at 230 °C for 4 h and then allowed to cool. The brown solid was extracted into methanol (500 mL) and stirred overnight, resulting in a brown solution and a white solid. The brown solution was separated by filtration and the volume reduced under vacuum conditions to precipitate a cream colored solid of hydrated 2,6-bis(2-benzimidazolyl)pyridine ($H_2BBP·0.5H_2O$) subsequently collected by filtration, washed with ether (2 × 10 mL), and air-dried (1.04 g, 16%). The water content was determined by NMR. ^1H NMR (300 MHz, 25 °C, $(CD_3)_2SO$): δ_H 12.99 (2H, s), 8.35 (2H, d), 8.18 (1H, t), 7.77 (4H, q), 7.33 (4H, m) and 3.30 (1H, s, H_2O) ppm. ^{13}C NMR (100.6 MHz, 25 °C, $(CD_3)_2SO$): δ 151.1, 148.1, 145.2, 141.0, 136.0, 125.1, 123.6, 121.2, 120.1, and 116.8 ppm. IR spectrum (Nujol): 737 (s), 742(s), 752(s), 766(m), 799(w), 821(s), 844(s), 889(w), 900(m), 927(m), 967(w), 958(m, sh), 964(s), 980(w), 992(m, sh), 995(s), 1010(s), 1073(m), 1111(w), 1121(w), 1127(w), 1145(w), 1149(w), 1154(m), 1166(w), 1174(w) cm^{-1}.

Synthesis of Water-Free 2,6-Bis(2-benzimidazolyl)pyridine, [H_2BBP·xPy]. In an inert atmosphere box, $H_2BBP·0.5H_2O$ (0.0950 g, 0.2966 mmol) was dissolved in pyridine (2 mL) and stirred over a mixture of 4 Å and 13X molecular sieves for 1 h, producing a cloudy solution. The solution was filtered through Celite supported on glass wool, and pentane (*ca.* 10 mL) was added with stirring to precipitate a white solid. The solid was collected by centrifugation, washed with pentane (3 × 1 mL), dried under vacuum conditions, and confirmed as the target $H_2BBP·0.5Py$ by NMR (0.101g, 97%). ^1H NMR (300 MHz, 25 °C, $(CD_3)_2SO$): δ_H 13.03 (2H, s), 8.61 (1H, d, Py), 8.39 (2H, d), 8.22 (1H, t), 7.85−7.75 (4.5H, brm), 7.45−7.30 (5H, brm) ppm. Analysis calculated for $C_{21.5}N_{5.5}H_{15.5}$: C, 73.59; N, 21.95; H, 4.45. Found: 73.60, 21.41, 4.56.

Synthesis of Monosodium 2,6-Bis(2-benzimidazolyl)-pyridine, [NaHBBP·xPy]. $H_2BBP·0.5Py$ (0.0163 g, 0.0464 mmol) and NaH (0.0006 g, 0.0250 mmol) were combined and stirred in pyridine (1 mL) for 60 min, producing a clear solution after initial bubbling. Pentane (5 mL) was added dropwise to the solution with stirring, leading to precipitation of a white solid collected by centrifugation, washed with ether (2 × 1 mL), dried under vacuum conditions (0.0157 g, 91%), and confirmed as $NaHBBP·0.5Py$ by NMR. ^1H NMR (300 MHz, 25 °C, $(CD_3)_2SO$): δ_H 13.08 (1H, s), 8.61 (1H, d, Py), 8.25 (2H, d), 8.01 (1H, t), 7.82(0.5H, t, Py), 7.62 (4H, m), 7.42 (1H, t, py), 7.10 (4H, m) ppm. The THF adduct can be formed by carrying out the reaction in THF to produce NaHBBP·xTHF.

Synthesis of Disodium 2,6-Bis(2-benzimidazolyl)pyridine, [Na_2BBP·xPy]. $H_2BBP·0.5Py$ (0.0084 g, 0.0239 mmol) and NaH (0.0011 g, 0.0500 mmol) were combined and stirred in pyridine (1 mL) for 60 min, producing a cloudy solution after initial bubbling. The solution was then centrifuged and the clear supernate collected. To the supernatant, pentane (5 mL) was added dropwise with stirring that resulted in the precipitation of a white solid collected by centrifugation, washed with ether (2 × 1 mL), dried under vacuum conditions (0.0089 g, 86%), and confirmed as $Na_2BBP·Py$ by NMR. ^1H NMR (300 MHz, 25 °C, $(CD_3)_2SO$): δ_H 8.57 (2H, d, Py) 8.16 (2H, d), 7.91 (1H, t), 7.78 (1H, t, Py), 7.53 (4H, m), 7.38(2H, t, Py), 6.97 (4H, m). The THF adduct can be formed by carrying out the reaction in THF to produce $Na_2BBP·x$THF.

Synthesis of 1, [UO_2(H_2BBP)Cl_2]. $H_2BBP·0.5Py$ (0.0245 g, 0.6980 mmol) and $UO_2Cl_2(THF)_3$ (0.0350 g, 0.0628 mmol) were stirred in pyridine (2 mL) for 1 h, producing a transparent yellow solution. Hexane (10 mL) was added dropwise to the solution with stirring to precipitate a yellow solid, collected on a medium porosity glass frit, washed with THF (2 × 1 mL), and dried under vacuum conditions (0.0401 g, 98%). ^1H NMR (300 MHz, 25 °C, $(CD_3)_2SO$): δ_H 13.11 (2H, s), 8.34 (2H, d), 8.18 (1H, t), 7.76 (4H, q), 7.33 (4H, m) ppm. Analysis calculated for $UO_2Cl_2C_{19}N_5H_{13}$: C, 34.99; N, 10.73; H, 2.01. Found; 35.70, 10.65, 1.94. IR spectrum (Nujol): 613(m), 625(m), 642(w), 662(w), 668(m), 675(w), 701(w), 722(s), 743(s), 765(m), 792(w), 802(m), 817(m), 847(m), 871(m), 888(w), 918(s), 930(s), 967(m), 998(s), 1005(s), 1018(w), 1034(m), 1045(w), 1064(m), 1078(w), 1117(m), 1147(m) 1153(m), 1191(w) cm^{-1}. Storage of a concentrated pyridine solution of **1** at −28 °C for several weeks yielded yellow block-like crystals of $[UO_2(BBP)Cl_2]·2Py$ suitable for X-ray diffraction.

Synthesis of 2, [UO_2(HBBP)(Py)Cl]·Py. NaHBBP·0.5Py (0.0303 g, 0.0812 mmol) in pyridine (1 mL) was added to a solution of $UO_2Cl_2(THF)_3$ (0.0403 g, 0.0723 mmol) in pyridine (1 mL) dropwise, producing a clear orange solution and was allowed to stir for 1 h. To the solution, pentane (6 mL) was added dropwise to precipitate an orange solid, collected by centrifugation, washed with THF (2 × 2 mL), and dried under vacuum conditions (0.0400 g, 71%). Analysis calculated for $UO_2ClC_{24}N_6H_{17}·Py$: C, 45.00; N, 12.66; H, 2.86. Found: 41.98, 11.85, 3.09. ^1H NMR of $[UO_2(BBP)(Py)Cl]·2Py$ (300 MHz, 25 °C, $(CD_3)_2SO$): δ_H 13.11 (1H, s), 8.61 (4H, d),

dx.doi.org/10.1021/ic4026359 | Inorg. Chem. 2014, 53, 2506−2515

Table 1. Crystal Data for Complexes 1−3

	compound **1**	compound **2**	compound **2a**	compound **3**
empirical formula	$C_{29}H_{23}Cl_2N_7O_2U$	$C_{29}H_{22}ClN_7O_2U$	$C_{56}H_{43}ClN_{13}O_2U$	$C_{29}H_{21}N_7O_2U$
fw	810.47	774.02	1203.51	737.56
temp (K)	150	150	150	150
cryst size (mm), color, shape	0.09	0.04	0.02	0.03
	0.06	0.04	0.02	0.03
	0.05	0.01	0.01	0.02
	green/yellow	orange	orange	red
	block	block	block	block
cryst syst, space group	monoclinic	monoclinic	triclinic	orthorhombic
	$P2(1)/n$	$P2(1)/c$	$p\bar{1}$	$Pbcn$
unit cell dimensions (Å)	a = 12.2371(9)	a = 14.4978(10)	a = 8.4712(7)	a = 13.7287(17)
	b = 18.0253(13)	b = 8.6973(6)	b = 14.8680(13)	b = 12.9878(16)
	c = 14.2323(10)	c = 21.3949(14)	c = 20.3713(18)	c = 14.8038(19)
unit cell angles (deg)	α = 90	α = 90	α = 80.382(2)	α = 90
	β = 115.091(2)	β = 101.319(2)	β = 81.000(2)	β = 90
	γ = 90	γ = 90	γ = 83.108(2)	γ = 90
cell volume (Å^3), Z	2843.1(4), 4	2645.2(3), 4	2486.9(4), 2	2639.6(6)
reflns collected/unique	40576/8643	39857/9074	66151/15129	26389/3860
	R(int) = 0.0648	R(int) = 0.0660	R(int) = 0.0433	R(int) = 0.0540
goodness-of-fit on F^2	1.039	1.084	1.022	1.049
final R indices [$I > 2\sigma(I)$]	R1 = 0.0305	R1 = 0.0377	R1 = 0.0267	R1 = 0.0270
	wR2 = 0.0794	wR2 = 0.0944	wR2 = 0.0583	wR2 = 0.0506
R indices (all data)	R1 = 0.0350	R1 = 0.0428	R1 = 0.0377	R1 = 0.0585
	wR2 = 0.826	wR2 = 0.0971	wR2 = 0.616	wR2 = 0.617

Scheme 1. Synthesis of 1−3

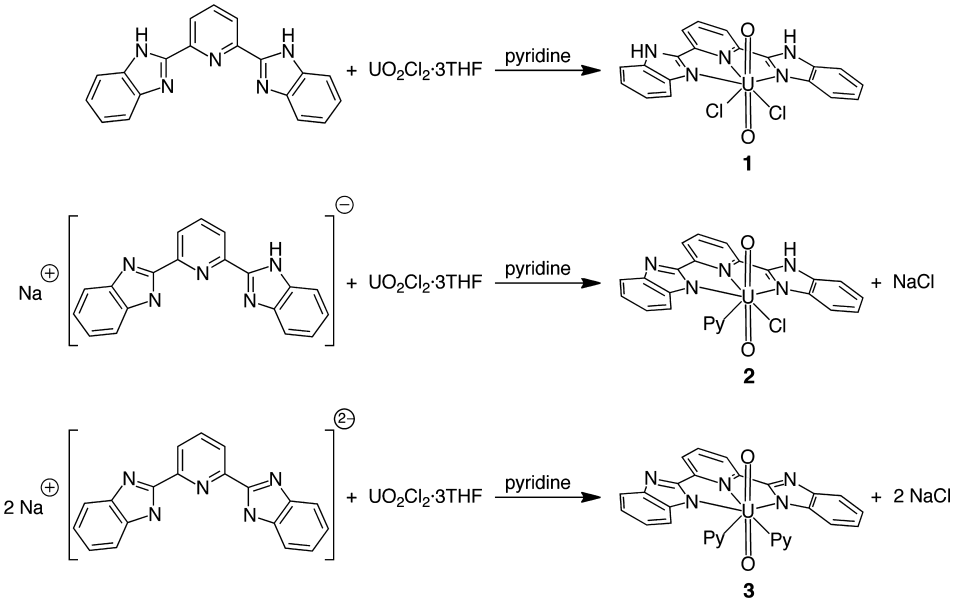

8.39 (2H, d), 8.22 (1H, t), 7.85−7.76 (6H, brm), 7.44−7.29 (8H, brm). IR spectrum (Nujol): 602(w), 627(m, sh), 631(m), 667(w), 673(w), 693(m), 707(m), 722(m), 729(m), 744(s), 749(s), 763(w), 793(w), 802(w), 825(m), 837(w), 849(m), 870(w), 905(w), 920(s, sh), 926(s), 957(w), 991(m), 1007(m), 1030(w, sh), 1035(m), 1041(w), 1041(w), 1067(m), 1083(w), 1117(w), 1142(w, sh) 1148(m) 1153(w), 1180(w) cm^{-1}. Evaporation of a pyridine/benzene solution of **2** overnight yielded crystals of [UO_2(BBP)(Py)Cl]·Py suitable for X-ray diffraction.

Synthesis of 3, [UO_2(BBP)(Py)$_2$]. Na_2BBP·Py (0.0057 g, 0.0131 mmol) was dissolved in pyridine (1 mL), to which $UO_2Cl_2(THF)_3$ (0.0070 g, 0.0126 mmol) in pyridine (1 mL) was added dropwise, producing a clear red solution and was allowed to stir for 1 h. To the solution, ether (5 mL) was added to precipitate a red solid, collected by centrifugation, washed with THF (2 × 1 mL), and dried under vacuum conditions (0.0078 g, 84%). ^{1}H NMR (300 MHz, 25 °C, $(CD_3)_2SO$): δ_H 9.25 (2H, d), 8.69 (2H, m), 8.59 (4H, t), 8.37 (2H, t), 7.79 (4H, t) 7.62 (1H, t), 7.31 (2H, t), 7.21 (4H, t). ^{1}H NMR (300 MHz, 25 °C, Py-D_5): 8.78 (2H, d), 8.20 (2H, d), 7.91 (1H, t), 7.81 (2H, t), 7.20 (4H, t), and Py-d_5 residual signals at 8.58, 7.42 and 7.06 ppm. Analytical calculated for $UO_2C_{29}N_7H_{21}$: C, 47.23; N, 13.29; H, 2.87. Found: 46.02, 13.39, 2.95. IR spectrum (Nujol): 630(m), 633(m, sh), 650(w), 674(m), 700(m), 709(w), 722(s), 736(w), 746(m), 755(w), 772(w), 790(w), 797(w), 825(m), 850(s), 880(w), 930(m), 939(m), 968(m), 995(m), 1009(w, sh), 1012(w, sh), 1039(w), 1041(w, sh), 1067(s), 1075(m), 1083(w), 1119(m), 1139(m)

dx.doi.org/10.1021/ic4026359 | Inorg. Chem. 2014, 53, 2506−2515

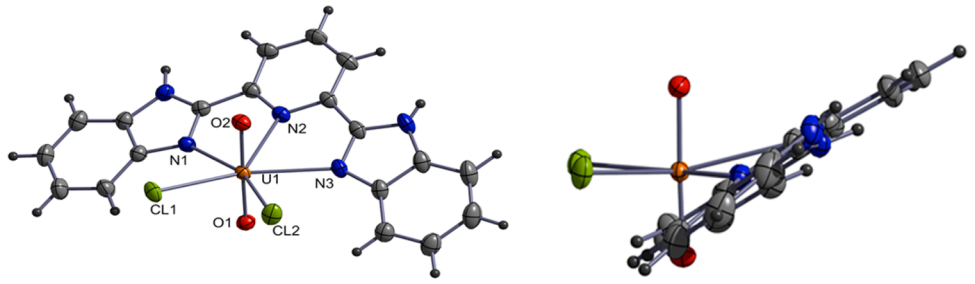

Figure 1. ORTEP (50% probability ellipsoids) representations of $[UO_2(H_2BBP)Cl_2]$ (**1**). The uranium atom is orange, chlorines yellow-green, oxygens red, nitrogens blue, and carbons gray.

1145(m, sh) 1155(w), 1162(w) cm^{-1}. Slow evaporation of a pyridine solution of **3** over several days yielded red cube-like crystals suitable for X-ray diffraction.

Crystallographic Data Collection and Refinement. All data were collected at 150 K on the Small Molecule X-ray Diffraction Beamline 11.3.1 Bruker ApexII diffractometer at the Advanced Light Source (ALS) of Lawrence Berkeley National Laboratory. The Bruker SADABS program was used for an empirical absorption correction, and all structures were solved by direct methods (SHELXS-97).[32] Crystallographic parameters for **1**−**3** are detailed in Table 1, and the crystallographic information files are available as Supporting Information (SI). Single crystals of **1**−**3** were transferred from the inert atmosphere glovebox in degassed paratone oil and mounted on a MicroMount before being transferred from the laboratory to the Beamline 11.3.1.

Scanning Transmission X-ray Microscopy. The Molecular Environmental Sciences (MES) Beamline 11.0.2 utilizes a Scanning Transmission X-ray Microscope (STXM) for NEXAFS at the light element thresholds and at the actinide $N_{IV,V}$ ($4d_{3/2,5/2}$) core level edges (700 to 940 eV) downstream of an elliptical polarization undulator (EPU). The STXM is downstream of a variable angle-included plane grating monochromator that is used routinely to collect NEXAFS spectra. The ALS-MES STXM can image and collect NEXAFS from particles with spatial resolution of better than 25 nm from ∼100 to 2000 eV.[33] The NEXAFS spectra are composed of transitions from element-specific electron core levels to unoccupied states, which yields both chemical and structural information.[34] Complexes **1**−**3** were prepared for STXM studies in an MBraun Labmaster 100 Ar-circulating glovebox. Minute amounts of powdered solids were transferred to a 100 nm thick Si_3N_4 window mounted on a STXM holder and hermetically sealed by the application of a second window with epoxy. Samples were transferred to the ALS-MES STXM in a sealed bottle and loaded into the STXM under a He gas stream. The STXM was dynamically purged with He to *ca.* 1 atm. The MES STXM data collection have been previously described in detail, and spectra from the complexes were extracted from image stacks (a set of registered images collected sequentially at each photon energy of a spectral scan).[35] The energy scale for U spectra was calibrated to the first absorption maximum of the Ne 1s to 3p transition at 867.3 eV. The assignment of spectral features is accurate to less than 0.1 eV. Uranium data were collected with horizontal EPU polarization (no polarization effects were observed), and all spectra were normalized to the incoming flux by integrating over the response from sample areas without particulates. All spectra have had a linear background subtracted and have been smoothed using a three or five point method excluding regions with sharp features.

RESULTS AND DISCUSSION

Synthesis and Structure of Uranyl BBP Complexes. The syntheses for complexes **1**−**3** are summarized in Scheme 1, and the simple syntheses of the base ligands are illustrated in Figure S1. The addition of H_2BBP to a solution of $UO_2Cl_2(THF)_3$ in pyridine at ambient temperature led to the formation of a yellow solution from which $[UO_2(H_2BBP)Cl_2]$ (**1**) in quantitative yield was isolated by precipitation with hexanes (Scheme 1, top). Storage of a pyridine solution of **1** at −28 °C for several weeks produced diffraction quality crystals that were structurally characterized as the molecular uranyl complex $[UO_2(H_2BBP)Cl_2]$ (**1**) (Figure 1). The complex contains one uranyl cation in a typical pentagonal bipyramidal geometry, coordinated to one H_2BBP ligand through two imidazole- and one pyridine-type nitrogen atom and to two chloride ligands in the equatorial plane. The H_2BBP ligand adopts nonplanar coordination geometry about the uranyl equatorial plane. The two chloride angles to uranyl at 93.68(7), 92.64(7), 88.11(7), and 88.25(8)° for O(1)−U(1)−Cl(1), O(1)−U(1)−Cl(2), O(2)−U(1)−Cl(1), and O(2)−U(1)−Cl(2), respectively, are close to ideal pentagonal bipyramidal geometry. The structural parameters exhibited by the H_2BBP ligand about uranyl can be referenced to an ideal equatorial coordination sphere about $\{UO_2\}^{2+}$ via a least-squares (LS) plane through U and the two Cl atoms. The N2 within the rigid H_2BBP deviates from this LS equatorial coordination sphere by 16.39° (Table 2). N1 and N3 sit slightly above and below the LS plane at angles of −3.77 and 0.87°, respectively. A calculated LS plane through the five N atoms within the planar and largely π conjugated H_2BBP ligand reveals a ligand deviation of 30.90° from the uranyl equatorial plane. The steric hindrance imposed by the uranyl moiety and the two Cl^- ligands are believed to be responsible for the deviation from equatorial planarity observed for the rigid H_2BBP ligand in **1**.

Table 2. Deviation of Ligands from Least Squares (LS) Plane in 1−3 (*Symmetry Generated Atom)

	1	2	2a	3
LS atoms	U1, Cl1, Cl2	U1, N6, Cl1	U1, N6, Cl1	U1, N1P, N1P*
N(1)	−0.168 Å, −3.77°	−0.514 Å, −11.43°	−0.1777 Å, −3.97°	0.0438 Å, 1.00°
N(2)	0.736 Å, 16.39°	0.208 Å, 4.64°	−0.3292 Å, −7.91°	0(0), 0°
N(3)	0.0389 Å, 0.87°	0.314 Å, 7.12°	0.1482 Å, 3.33°	−0.0438 Å, 1.00°
LS BBP N atoms atoms	30.90°	13.20°	12.89°	3.50°

Deprotonation of the free base BBP (H_2BBP) and the successive reaction of the newly synthesized ligand salt NaHBBP with uranyl chloride in pyridine yields an orange solution from which $[UO_2(HBBP)ClPy]$(**2**) (80%) was obtained by the addition of pentane and crystallized from a pyridine/benzene mix (Scheme 1, center). The resultant loss of NaCl leads to the insertion of pyridine into the uranyl equatorial coordination sphere in **2** (Figure 2). The loss of

dx.doi.org/10.1021/ic4026359 | Inorg. Chem. 2014, 53, 2506−2515

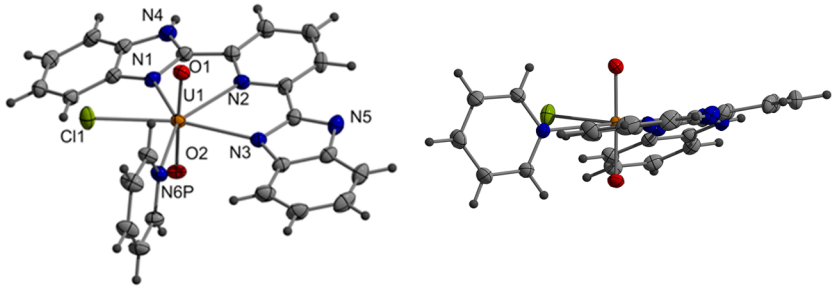

Figure 2. ORTEP (50% probability ellipsoids) representations of $[UO_2(HBBP)ClPy]$ (**2**). The uranium atom is orange, chlorine yellow-green, oxygens red, nitrogens blue, and carbons gray.

Table 3. Bond Distances (Å) and Angles (deg) for Complexes 1−3 (*Symmetry Generated and (m) Measured in Crystallographic Representation Software)

1		2		2a	3	
U(1)−(O1)	1.765(2)	U(1)−O(1)	1.762(3)	1.7563(18)	U(1)−O(1)	1.768(4)
U(1)−(O2)	1.772(2)	U(1)−O(2)	1.773(3)	1.7632(18)	U(1)−O(1A) *	1.768(4)
U(1)−N(1)	2.555(2)	U(1)−N(1)	2.593(4)	2.568(2)	U(1)−N(1)	2.501(4)
U(1)−N(2)	2.607(3)	U(1)−N(2)	2.573(4)	2.5622(18)	U(1)−N(2)	2.519(7)
U(1)−N(3)	2.579(3)	U(1)−N(3)	2.533(4)	2.553(2)	U(1)−N(1A)*	2.501(7)
U(1)−Cl(1)	2.6606(8)	U(1)−N(6)	2.554(4)	2.523(2)	U(1)−N(1P)	2.538(4)
U(1)−Cl(2)	2.6914(8)	U(1)−Cl(1)	2.6854(12)	2.6832(7)	U(1)−N(1PA)*	2.538(4)
O(1)−U(1)−O(2)	178.10(10)	(O1)−U(1)−(O2)	176.53(14)	177.08(9)	(O1)−U(1)−(O2)	176.2(2)
O(1)−U(1)−N(1)	84.83(9)	O(1)−U(1)−N(1)	97.82(13)	88.58(8)	O(1)−U(1)−N(1)	90.84(17)
O(1)−U(1)−N(2)	102.24(9)	O(1)−U(1)−N(2)	85.36(13)	94.95(7)	O(1)−U(1)−N(2)	91.89(11)
O(1)−U(1)−N(3)	88.22(9)	O(1)−U(1)−N(3)	86.61(14)	88.63(8)	O(1)−U(1)−N(1)*	90.69(17)
O(1)−U(1)−Cl(1)	93.68(7)	O(1)−U(1)−Cl(1)	87.41(11)	94.30(6)	O(1)−U(1)−N(1P)	87.77(15)
O(1)−U(1)−Cl(2)	92.64(7)	O(1)−U(1)−N(6)	92.26(13)	89.50(8)	O(1)−U(1)−N(1P)*	89.08(15)
O(2)−U(1)−N(2)	76.00(9)	O(2)−U(1)−N(2)	95.34(13)	84.47(7)	N(1P)−U(1)−N(1)	80.19(14)
O(2)−U(1)−N(1)	94.92(9)	O(2)−U(1)−N(1)	85.53(13)	93.73(8)	N(1)−U(1)−N(2)	66.10(10)
O(2)−U(1)−N(3)	90.33(9)	O(2)−U(1)−N(3)	90.58(14)	88.53(7)	N(2)−U(1)−N(1)*	66.10(10)
O(2)−U(1)−Cl(1)	88.12(7)	O(2)−U(1)−Cl(1)	94.17(11)	87.81(6)	N(1)*−U(1)−N(1P)*	80.19(14)
O(2)−U(1)−Cl(2)	88.22(8)	O(2)−U(1)−N(6)	85.26(13)	89.23(63)	N(1P)−U1−N(1P)*	67.43(19)
Cl(1)−U(1)−Cl(2)	80.76(3)	Cl(1)−U(1)−N(6)	72.74(9)	71.76(5)	N(1)−N(2)−N(1)*	114.94(m)
Cl(1)−U(1)−N(1)	80.26(6)	Cl(1)−U(1)−N(1)	78.91(8)	81.73(4)		
N(1)−U(1)−N(2)	62.54(8)	N(1)−U(1)−N(2)	63.76(12)	64.30(6)		
N(2)−U(1)−N(3)	62.73(8)	N(2)−U(1)−N(3)	65.48(12)	64.84(6)		
N(3)−U(1)−Cl(2)	77.32(6)	N(3)−U(1)−N(6)	80.79(12)	78.08(7)		
N(1)−N(2)−N(3)	113.0(m)	N(1)−N(2)−N(3)	114.43(m)	114.94(m)		

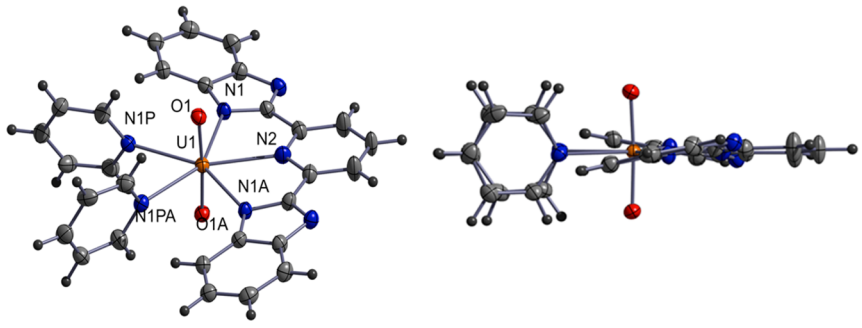

Figure 3. ORTEP (50% probability ellipsoids) representations of $[UO_2(BBP)Py_2]$ (**3**). The uranium atom is orange, oxygens red, nitrogens blue, and carbons gray.

chloride and concomitant coordination of pyridine decreases the steric constraints about uranyl and results in the ligand adopting a closer to planar coordination geometry than observed in **1** and indicated by an angle of 13.20° cast between the LS plane through U1, Cl1, and N6 and the BBP ligand. The Cl^- and pyridine ligands adopt coordination angles close to ideal equatorial geometry with uranyl at 87.41(11) and 92.26(13)°, respectively (Table 3). The N2 ligand of BBP resides at 4.64° above the ideal uranyl equatorial plane, and the flanking N1 and N3 imidazole nitrogen donor atoms are at −11.43 and 7.12°, respectively, which are greater than those observed in **1** and indicate a greater distortion of the overall

dx.doi.org/10.1021/ic4026359 | Inorg. Chem. 2014, 53, 2506−2515

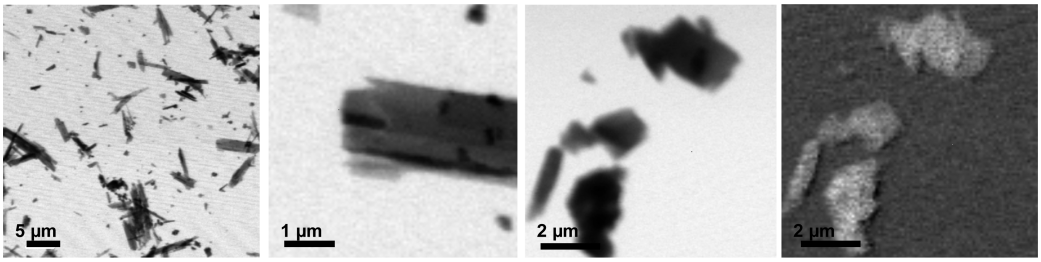

Figure 4. Four representative images recorded from the STXM investigations of complexes **1**−**3** at ALS-MES Beamline 11.0.2. From left to right, two normal contrast X-ray images of crushed single crystals obtained with a photon energy of 398 eV, a normal contrast image taken at 737.5 eV of a crushed precipitate, and a U elemental map of these corresponding particulates examined from the crushed precipitate.

ligand planarity. The structural parameters and ligand geometry in **2** can be influenced by additional groups H-bonding to the exterior noncoordinating BBP N atoms as was observed in **2a** (see SI Figure S4). Complex **2a** which contains an additional H_2BBP molecule H-bonded to the exterior N5 through two imidazole protons was crystallized from a solution containing excess ligand. While the molecular complex in **2a** $[UO_2(HBBP)ClPy]$ is identical to **2**, the molecular geometry is slightly different (Table 3). The BBP ligand retains a similar displacement from equatorial planarity and exhibits a 12.89° angle between two LS planes through U1, N6, and Cl1 and the nitrogen atoms of the BBP ligand similar to that observed in **2**. However, the coordinated nitrogen atoms reside from the equatorial plane at angles of −3.97, −7.91, and 3.33° for N1, N2, and N3, respectively (Table 2), indicating that the ligand planarity is not as distorted as in **2**, a result of the additional H-bonding H_2BBP molecule and resulting crystal packing.

The addition of the doubly deprotonated BBP ligand (Na_2BBP) to uranyl chloride in pyridine leads to the formation of a red solution from which $[UO_2(BBP)Py_2]$ (**3**) can be isolated by the addition of ether (84%) and crystallized by slow evaporation (Scheme 1, bottom). In **3** (Figure 3), the two uranium-coordinating chlorides have been replaced by two pyridine ligands following the loss of two equivalents of NaCl. The complex is pentagonal bipyramidal exhibiting a nearly ideal planar equatorial coordination sphere about uranyl and having a center of symmetry through U1. The coordinating pyridine ligands have N1P−U1−O1 and N1PA−U1−O1 angles close to ideal pentagonal bipyramidal geometry at 87.77(15) and 89.08(15)°. A calculated LS plane generated through the uranium atom and two coordinated pyridine nitrogen atoms (N1P, N1PA, and U1) reveals that the BBP N2 atom in **3** resides at ideal equatorial planarity (Table 2). The two flanking BBP nitrogen atoms (N1 and N1A) also sit close to equatorial planarity at 1° above and below this plane, respectively. A LS plane through the ligand nitrogen atoms reveals a displacement angle of 3.5° from the equatorial uranyl LS plane. The loss of the two Cl^- ligands from the $\{UO_2\}^{2+}$ equatorial plane presumably relaxes the steric restrictions, allowing the BBP ligand to occupy a coordination environment very close to planar. A detailed comparison of bond distances and angles for compounds **1**−**3** is given in Table 3.

As the charge on the BBP ligand changes from 0 to −2 in **1**−**3**, the coordination geometry to uranyl becomes tighter with average BBP coordinating nitrogen uranyl distances of 2.580(26), 2.566(30), and 2.505(10) Å for **1**−**3**, respectively. While the average distance is within error for **1** and **2**, the centrally coordinating N2 nitrogen decreases in bond distance from 2.606(3) and 2.573(4) to 2.519(7) Å for **1**, **2**, and **3**, respectively. There is also a noticeable decrease in the shortest flanking U−N bond distance from **1**−**3** upon inspection of metrical parameters (Table 3). The shorter distances are attributed to an increased interaction of ligand through the elevation of charge and steric considerations as the coordination ligands are replaced through metathesis of the chloride. The increased ligand interaction in the equatorial plane results in a distortion of the O═U═O bond angle from the ideal linearity of 180° with angles of 178.11(10)°, 176.53(14)°, and 176.2(2)° observed for **1**−**3**, respectively, and are typical for the uranyl cation. However, the uranyl U═O distances in **1**−**3** exhibit little deviation from each other and range from 1.7563(18) Å to 1.773(3) Å, which are typical for the uranyl cation in N-donor environments.[16,20,36] The decrease in bond distance between BBP and uranium in **1**−**3** and the deviation of the uranyl bond from linearity suggests a slight weakening of the uranyl bonds as the ligand becomes more electron rich and the electron withdrawing chlorides are removed, thus increasing electron donation from the ligand through the uranyl equatorial plane. Vibrational spectroscopy can be used to measure the strength of the uranyl bond via the uranyl asymmetric stretching frequency, and therefore, complexes **1**−**3** were probed by IR spectroscopy. However, the data were inconclusive, and the asymmetric ν_3(O═U═O) stretch could not be identified from interfering stretch modes from the BBP ligand. Weak IR bands are apparent in **1**−**3** at 792, 793, and 790 cm^{-1}, respectively, which are assigned to the ν_1(O═U═O) stretching vibration and indicative of a deviation from linearity within the $\{UO_2\}^{2+}$ moiety.

Scanning Transmission X-Ray Microscopy. A recent approach to exploring the electronic properties of actinide and lanthanide complexes has been by use of a STXM, utilizing soft X-ray synchrotron radiation to probe the light atom 1s and metal 2p, 3d, and 4d edges by Near-Edge X-ray Absorption Fine Structure (NEXAFS).[37−41] NEXAFS spectra obtained from STXM measurements are interpreted to identify solid state structure and oxidation state and can directly probe the light atom bonding characteristics as has been done for a related BBP complex.[39] The STXM at the ALS-MES Beamline 11.0.2 has successfully investigated $[(CpSiMe_3)U\text{-}AlCp^*]$ (Cp = C_5Me_5), $[U((H_2BBP)_3]Cl_4$, and layered lanthanide and actinide chalcogenide extended solids (e.g., $La_2U_2Se_9$ and $Tl_3Cu_4USe_6$), as well as evaluating covalence in transition metal oxygen multiple bonds.[37−40,42] These studies provide insight into bonding, electronic structure, oxidation state, and solid-state geometry in f-element complexes. Given the structural and geometric differences in complexes **1**−**3**, the U 4d-edges were probed by STXM NEXAFS spectroscopy to investigate any influence the differing coordination environments might have on the local electronic structure in **1**−**3** by NEXAFS. The imaging capabilities of the STXM are illustrated in Figure 4. An

dx.doi.org/10.1021/ic4026359 | Inorg. Chem. 2014, 53, 2506−2515

elemental map of each particle was taken prior to NEXAFS spectrum collection to ensure uranium homogeneity in the sample. Examination of each particle in this manner prior to recording NEXAFS spectra confirmed that the compounds are uniform in composition and show no signs of degradation from the exposure to atmosphere or the soft X-ray beam.

The U 4d-edge NEXAFS spectra from **1**−**3** is shown in Figure 5. The uranium NEXAFS spectra for **1**−**3** are composed

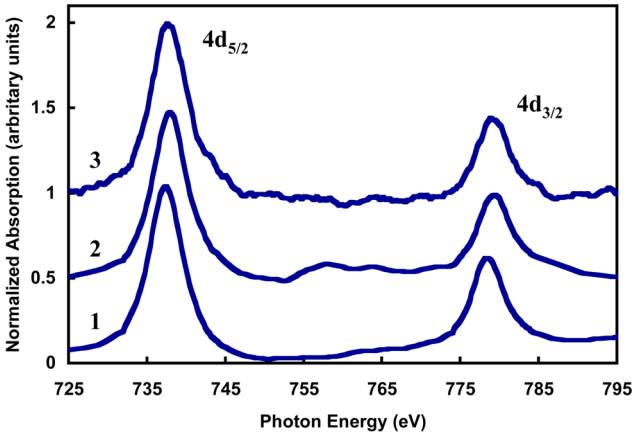

Figure 5. Uranium $N_V(4d_{5/2})$- and $N_{IV}(4d_{3/2})$-edge NEXAFS spectra collected from complexes **1**−**3**.

of two main features, the U $4d_{5/2}$ (N_V) and U $4d_{3/2}$ (N_{IV}) transitions. The transitions from the U 4d orbitals primarily probe unoccupied states with U 5f character.[43] The $4d_{5/2}$ transition is primarily utilized to ascertain the oxidation state on the uranium center through the charge state shift and in conjunction with the $4d_{3/2}$ transition can at times provide additional bonding characteristics.[41,43] The maxima for the $4d_{5/2}$ edge energies are at 737.4, 738.0, and 737.7 eV and $4d_{3/2}$ energies at 778.5, 779.4, and 778.9 eV for **1**−**3**, respectively. These transition energies are higher than those measured recently in U(III), U(IV), and potentially U(V) containing compounds and indicative of a higher oxidation state.[37−40] Literature data are limited on U 4d edge energies, but the range observed for **1**−**3** is slightly below that previously recorded for the U(VI) containing material Schoepite, $(UO_2)O(OH)_6 \cdot 6H_2O$ ($4d_{5/2}$ at 738.4 eV), and is similar to those of other uranyl(VI) containing materials.[37,41] There is no clear trend in the transition energies from the NEXAFS spectra of the complexes that can be correlated to overall electron donating/withdrawing character of the coordinating BBP ligand and substituents of complexes **1**−**3** within experimental resolution. The small energy differences could suggest subtle differences in bonding and electronic structure. The transition energies observed in **1**−**3** and characterization of the U(VI) oxidation state confirms that no redox activity is encountered between BBP and the uranium center. It is worth noting that the branching ratio ($4d_{5/2}/4d_{3/2}$) derived from the peak intensities in **1**−**3** are similar. The broad feature between the uranium 4d white line transitions in **1**−**3** that is more pronounced in **2** is a feature observed in other uranium 4d spectra, but has yet to be assigned.

First-Principles Geometry Optimization. The uranyl complexes **1**−**3** have been investigated using the first-principles DFT-based electronic structure code, VASP (Vienna *ab initio* simulation package).[44−46] The calculations employed a plane wave basis with PAW (Projector Augmented Wave) pseudopotentials within the LDA (Local Density Approximation) for the exchange-correlation potential.[46−49] In the calculations, a 2 × 2 × 2 k-point grid was used and a 500 eV cutoff energy for the wave functions.[50] The LDA typically gives a poor description of f-electron systems such as bulk uranium but in uranyl, the uranium is nominally hexavalent, so there is little occupied f-electron character and LDA can give a good description of the electronic ground state. It was also found that adding an on-site Hubbard (+U) correction to the LDA potential, which is often used to give a better description of f electrons, yielded similar results to LDA.

The three compounds **1**−**3** were simulated to confirm and validate the experimental structures of the complexes. On the basis of the crystallographic data of atomic/molecular positions, relaxation tests were done with fixed lattice vectors. The atomic positions were relaxed until the forces were below 0.01 eV/Å. Several typical bond distances and angles are listed in Table 4 for the relaxed structures compared to the experimental values. As shown in Table 4, the calculated values of bond distances agree to within a few percent of the experimental values while also reproducing observed trends across the different compounds. For example, the average U to BBP N bond-distances shows a decreasing trend in compounds **1**, **2**, **2a**, and **3** at 2.552 Å (2.581 Å), 2.543 Å (2.566 Å), 2.534 Å (2.561 Å), and 2.488 Å (2.507 Å) within both theory and experiment, respectively. Within LDA, the strongly covalent uranyl U═O bond distances seem to be systematically overestimated by ∼1.7%, while the weaker U−N dative distances are underestimated by ∼1%. The angle between the equatorial plane and

Table 4. Electronic Structure Calculation Results for Crystal Structure Parameters and Comparison to Experimental Results Given in Parentheses[a]

compound **1**		compound **2**		**2a**	compound **3**	
bond	distance (Å)/angle (deg)	bond	distance (Å)/angle (deg)		bond	distance (Å)/angle (deg)
U−O(1)	1.797 (1.766)	U−O(1)	1.786 (1.762)	1.794 (1.7563)	U−O(1)	1.794 (1.768)
U−O(2)	1.794 (1.772)	U−O(2)	1.792 (1.773)	1.792 (1.7632)	U−O(2)	1.794 (1.768)
U−N(1)	2.524 (2.556)	U−N(1)	2.566 (2.593)	2.532 (2.568)	U−N(1)	2.485 (2.501)
U−N(2)	2.581 (2.606)	U−N(2)	2.547 (2.573)	2.544 (2.5622)	U−N(2)	2.495 (2.519)
U−N(3)	2.552 (2.581)	U−N(3)	2.516 (2.533)	2.527 (2.553)	U−N(3)	2.485 (2.501)
U−Cl(1)	2.633 (2.661)	U_N(6)	2.518 (2.554)	2.496 (2.523)	U−N(P1)	2.503 (2.538)
U−Cl(2)	2.672(2.692)	U−Cl(1)	2.657 (2.6854)	2.643 (2.6832)	U−N(P2)	2.503 (2.538)
O═U═O	178.7 (178.1)	O═U═O	176.04 (176.53)	175.47 (177.08)	O═U═O	175.0 (176.2)
†eq/N(2)	14.8 (18.2)	†eq/N(2)	4.99 (4.64)	−8.59 (−7.91)	†eq/N(2)	0.0 (0.0)

[a]The equatorial plane was generated using Cl(1)−U−Cl(2), Cl(1)−U−N(6), or N(P1)−U−N(P2) surfaces.

dx.doi.org/10.1021/ic4026359 | Inorg. Chem. 2014, 53, 2506−2515

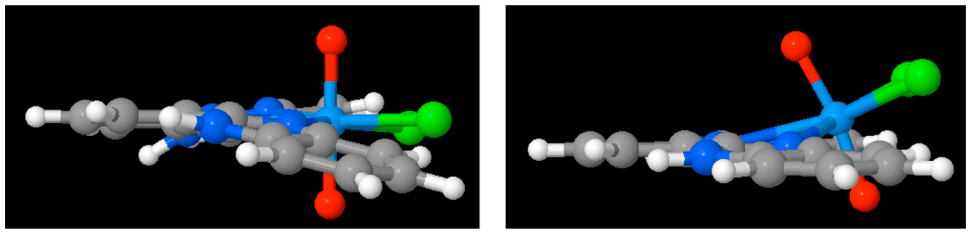

Figure 6. Geometry of an isolated molecule of complex **1** before and after first-principles structural optimization starting from a nearly planar structure (left and right, respectively). The uranium atom is light blue, chlorine green, oxygens red, nitrogens blue, and carbons gray.

the N2 site is underestimated for compound **1** and slightly overestimated for compound **2**. Nevertheless, we observe the overall trend of a higher nonplanar angle for compound **1** than the other compounds. From the calculations, the variation in total energy with this angle was found to be small. Theory also reproduces the experimentally observed trend in the O═U═O bond angle within the complexes with increasing nonlinearity going from **1** to **3**.

The experiments and the electronic structure calculations for compounds **1** and **2** yield distinct out-of-plane bonding between uranyl and the BBP ligands. The objective of the asymmetry analysis was to determine if the asymmetry is only present in the crystal and not in the isolated molecule and to determine if it results from a steric effect in the isolated molecule or by lowering the energy of the crystal. The stability of the planar structure for the crystal was investigated by starting with the chlorines in the BBP plane followed by atomic relaxation and observations of how the atoms moved to see if the planar structure is a metastable state. From this simulation, it was found that the complex relaxes back to the asymmetric out-of-plane structure. The second evaluation was to construct a supercell for an isolated molecule with 10 Å of vacuum space in all directions and relax this system to see if the out-of-plane structure is also stable for the isolated molecule. Similar to the previously described simulation, a single molecule of compound **1** was configured as a flat ligand structure with the uranium and chlorine atoms in the plane of BBP. The flat structure version of compound **1** was created from compound **3** by replacing the pyridines with Cl and adding two H atoms bonded to the N4 and N5 nitrogen sites. As the system was relaxed, the uranyl unit and chlorine atoms reposition to a similar angle as the experimental crystal structure (see Figure 6), which is evidence that the out-of-plane structure is not driven by crystal formation. The flat structure was also relaxed but keeping the uranium and chlorine atoms constrained to reside in the plane of BBP to compare to the fully relaxed out-of-plane single complex structure. It was found that the nonplanar geometry was 0.116 eV lower in energy than the constrained planar geometry. Relevant structural parameters for the two systems are reported in Table S2 of the Supporting Information. We find that relative to the planar structure, the nonplanar structure exhibits U−N1 and U−N3 bonds that are ∼2.5% shorter while the U−N2 bond is virtually unchanged (2.642 Å for the planar case and 2.650 Å for the nonplanar geometry). The shorter U−N1 and U−N3 bonds are facilitated by a small buckling of the H_2BBP ligand in the nonplanar structure as evidenced by the smaller included angle ∠N1−N2−N3 of 113.7° as compared to 117.8° in the planar structure. Such a buckling of the ligand is precluded in the planar configuration resulting from the steric interaction between the chlorines and the benzimidazole groups of the H_2BBP ligand. In contrast, the almost planar complex **3** exhibits both shorter U−N bond lengths (see Table 4) as well as a ∠N1−N2−N3 angle of 113.5°, which suggests that a similar steric interaction is not present between pyridine ligands and the benzimidazole groups of the BBP ligand.

To determine if the different BBP coordination angles in the uranyl equatorial plane in **1**−**3** could be influenced by the overall BBP charge, as well as coordinating chloride ligands, the isolated complexes were studied with substitution of different halides F^-, Br^-, and I^- for Cl^- ligands. The out-of-plane angles were found to vary greatly with the different halides, with larger halide ionic radii leading to larger out-of-plane angles, further suggesting steric effects predominantly control the coordination angle.

CONCLUDING REMARKS

Synthesis of the mononuclear molecular uranyl complexes, **1**−**3**, was achieved by first synthesizing water free H_2BBP ligand derivatives and single and double deprotonated sodium salts. The BBP derivatives are capable of displacing chloride ligands from the uranyl equatorial plane by controlled salt methathesis reactions in pyridine. The structural differences observed for **1**−**3** and the tendency for the tridentate ligand to adopt an out of plane angle about uranyl is a direct result of the bulky coordinating chloride ligands. Relaxation of the steric constraints by replacement of chloride with a pyridine ligand allows the tridentate BBP ligand to adopt a geometry closer to equatorial planarity about the uranyl cation. As the BBP becomes increasingly charged, it also adopts tighter coordination geometry about uranyl as indicated by a reduction in the average U−N bond distances in **1**−**3**. The STXM NEXAFS at the U 4d edges confirms the hexavalent uranyl nature of the BBP complexes; however, STXM NEXAFS cannot firmly establish electron donation or withdrawal effects within the series of BBP complexes by use of the U 4d edge transition energies. The first-principles theoretical results substantiate the bond distances and angles obtained from experimental measurements and establish that steric effects drive the out-of-plane bonding.

ASSOCIATED CONTENT

Supporting Information

Supporting figures pertaining to the syntheses of the base ligands, NMR and IR spectra for **1**−**3** and base ligands, alternative ORTEP representations of complex **2**−**2a**, atomic coordinates for X-ray crystallographic data and from theory for complexes **1**−**3**, X-ray crystallographic data in .cif format, and a table of optimized structural parameters from theory for an isolated molecular unit of complex **1**. This material is available free of charge via the Internet at http://pubs.acs.org.

dx.doi.org/10.1021/ic4026359 | *Inorg. Chem.* 2014, 53, 2506−2515

AUTHOR INFORMATION

Corresponding Authors

*E-mail: Copping@lanl.gov.
*E-mail: ACanning@lbl.gov.
*E-mail: DGPrendergast@lbl.gov.
*E-mail: DKShuh@lbl.gov.

Present Addresses

▽Inorganic, Isotope and Actinide Chemistry Group (C-IIAC), Los Alamos National Laboratory, Los Alamos, NM 87545, United States
○School of Engineering and Applied Sciences, Harvard University, Cambridge, MA 02138, United States

Notes

The authors declare no competing financial interest.

ACKNOWLEDGMENTS

The research was supported by the Laboratory Directed Research and Development Program of Lawrence Berkeley National Laboratory (LBNL) and as a User Project at the Molecular Foundry, LBNL, both under U.S. Department of Energy Contract No. DE-AC02-05CH11231. Calculations were performed on the Cray XE6 Hopper computer at the National Energy Research Scientific Computing Center (NERSC-LBNL) and Molecular Foundry computing resources, Nano and Vulcan, managed by the High Performance Computing Services Group of LBNL. The research at the Molecular Environmental Sciences Beamline 11.0.2 at the Advanced Light Source (ALS) was supported by the U.S. Department of Energy, Director, Office of Science, Division of Chemical Sciences, Geosciences, and Biosciences at LBNL under Contract DE-AC02-05CH11231. The ALS, research at Beamline 11.3.1, ST, and TT were supported by the U.S. Department of Energy, Director, Office of Science, Office of Basic Energy Sciences at LBNL under Contract DE-AC02-05CH11231. We also thank Sean D. Reilly at Los Alamos National Laboratory for Chemdraw synthetic schemes.

REFERENCES

(1) Berthet, J. C.; Lance, M.; Nierlich, M.; Ephritikhine, M. *Eur. J. Inorg. Chem.* **2000**, 1969−1973.
(2) Berthet, J. C.; Nierlich, M.; Ephritikhine, M. *Chem. Commun.* **2004**, 870−871.
(3) Burns, C. J.; Clark, D. L.; Donohoe, R. J.; Duval, P. B.; Scott, B. L.; Tait, C. D. *Inorg. Chem.* **2000**, *39*, 5464−5468.
(4) Wilkerson, M. P.; Burns, C. J.; Paine, R. T.; Scott, B. L. *Inorg. Chem.* **1999**, *38*, 4156.
(5) Bart, S. C.; Meyer, K. Highlights in uranium coordination chemistry. In *Organometallic and Coordination Chemistry of the Actinides*; Albrecht-Schmitt, T. E., Ed.; Springer: New York, 2008; Vol. *127*, pp 119−176.
(6) Ephritikhine, M. *Dalton Trans.* **2006**, 2501−2516.
(7) Jones, M. B.; Gaunt, A. J. *Chem. Rev.* **2012**, *113*, 1137−1198.
(8) *The Chemistry of the Actinide and Transactinide Elements*; Morss, L. R., Edelestein, N. M., Fuger, J., Eds.; Springer: Dordrecht, The Netherlands, 2006.
(9) Arnold, P. L.; Love, J. B.; Patel, D. *Coord. Chem. Rev.* **2009**, *253*, 1973−1978.
(10) Fortier, S.; Hayton, T. W. *Coord. Chem. Rev.* **2010**, *254*, 197−214.
(11) Hayton, T. W. *Chem. Commun.* **2013**, *49*, 2956−2973.
(12) Baker, R. J. *Chem.—Eur. J.* **2012**, *18*, 16258−16271.
(13) Cantat, T.; Arliguie, T.; Noel, A.; Thuery, P.; Ephritikhine, M.; Le Floch, P.; Mezailles, N. *J. Am. Chem. Soc.* **2009**, *131*, 963−972.
(14) Maynadie, J.; Berthet, J. C.; Thuery, P.; Ephritikhine, M. *Chem. Commun.* **2007**, 486−488.
(15) Berthet, J. C.; Nierlich, M.; Ephritikhine, M. *Dalton Trans.* **2004**, 2814−2821.
(16) Berthet, J. C.; Thuery, P.; Dognon, J. P.; Guillaneux, D.; Ephritikhine, M. *Inorg. Chem.* **2008**, *47*, 6850−6862.
(17) Berthet, J. C.; Thuery, P.; Ephritikhine, M. *Chem. Commun.* **2007**, 604−606.
(18) Sarsfield, M. J.; Helliwell, M. *J. Am. Chem. Soc.* **2004**, *126*, 1036−1037.
(19) Sarsfield, M. J.; Helliwell, M.; Collison, D. *Chem. Commun.* **2002**, 2264−2265.
(20) Sarsfield, M. J.; Helliwell, M.; Raftery, J. *Inorg. Chem.* **2004**, *43*, 3170−3179.
(21) Sarsfield, M. J.; Steele, H.; Helliwell, M.; Teat, S. J. *Dalton Trans.* **2003**, 3443−3449.
(22) Sessler, J. L.; Melfi, P. J.; Pantos, G. D. *Coord. Chem. Rev.* **2006**, *250*, 816−843.
(23) Barnhart, D. M.; Burns, C. J.; Sauer, N. N.; Watkin, J. G. *Inorg. Chem.* **1995**, *34*, 4079−4084.
(24) Drew, M. G. B.; Hill, C.; Hudson, M. J.; Iveson, P. B.; Madic, C.; Vaillant, L.; Youngs, T. G. A. *New J. Chem.* **2004**, *28*, 462−470.
(25) Escande, A.; Guenee, L.; Buchwalder, K.-L.; Piguet, C. *Inorg. Chem.* **2009**, *48*, 1132−1147.
(26) Muller, G.; Bunzli, J. C. G.; Schenk, K. J.; Piguet, C.; Hopfgartner, G. *Inorg. Chem.* **2001**, *40*, 2642−2651.
(27) Petoud, S.; Bunzli, J. C. G.; Glanzman, T.; Piguet, C.; Xiang, Q.; Thummel, R. P. *J. Lumin.* **1999**, *82*, 69−79.
(28) Petoud, S.; Bunzli, J. C. G.; Schenk, K. J.; Piguet, C. *Inorg. Chem.* **1997**, *36*, 1345−1353.
(29) Piguet, C.; Bunzli, J. C. G.; Bernardinelli, G.; Hopfgartner, G.; Williams, A. F. *J. Am. Chem. Soc.* **1993**, *115*, 8197−8206.
(30) Kolarik, Z. *Chem. Rev.* **2008**, *108*, 4208−4252.
(31) Addison, A. W.; Burke, P. J. *J. Heterocycl. Chem.* **1981**, *18*, 803−805.
(32) Sheldrick, G. M. *Acta Crystallogr., Sect. A* **2008**, *64*, 112−122.
(33) Bluhm, H.; Andersson, K.; Araki, T.; Benzerara, K.; Brown, G. E.; Dynes, J. J.; Ghosal, S.; Gilles, M. K.; Hansen, H. C.; Hemminger, J. C.; Hitchcock, A. P.; Ketteler, G.; Kilcoyne, A. L. D.; Kneedler, E.; Lawrence, J. R.; Leppard, G. G.; Majzlan, J.; Mun, B. S.; Myneni, S. C. B.; Nilsson, A.; Ogasawara, H.; Ogletree, D. F.; Pecher, K.; Salmeron, M.; Shuh, D. K.; Tonner, B.; Tyliszczak, T.; Warwick, T.; Yoon, T. H. *J. Electron Spectrosc. Relat. Phenom.* **2006**, *150*, 86−104.
(34) Stohr, J. *NEXAFS Spectroscopy*: Springer-Verlag: Berlin, 2003.
(35) Hitchcock, A. P.; Araki, T.; Ikeura-Sekiguchi, H.; Iwata, N.; Tani, K. J. *Phys. IV France* **2003**, *104*, 509−512.
(36) Berthet, J. C.; Thuery, P.; Foreman, M. R. S.; Ephritikhine, M. *Radiochim. Acta* **2008**, *96*, 189−197.
(37) Bugaris, D. E.; Choi, E. S.; Copping, R.; Glans, P. A.; Minasian, S. G.; Tyliszczak, T.; Kozimor, S. A.; Shuh, D. K.; Ibers, J. A. *Inorg. Chem.* **2011**, *50*, 6656−6666.
(38) Bugaris, D. E.; Copping, R.; Tyliszczak, T.; Shuh, D. K.; Ibers, J. A. *Inorg. Chem.* **2010**, *49*, 2568−2575.
(39) Janousch, M.; Copping, R.; Tyliszczak, T.; Castro-Rodriguez, I.; Shuh, D. K. Scanning transmission x-ray spectromicroscopy of actinide complexes. In *Actinides 2008 - Basic Science, Applications and Technology*; Shuh, D. K., Chung, B. W., Albrecht-Schmitt, T., Gouder, T., Thompson, J. D., Eds.; Materials Research Society: Warrendale, PA, 2008; Vol. *1104*, pp 165−170.
(40) Minasian, S. G.; Krinsky, J. L.; Rinehart, J. D.; Copping, R.; Tyliszczak, T.; Janousch, M.; Shuh, D. K.; Arnold, J. *J. Am. Chem. Soc.* **2009**, *131*, 13767−13783.
(41) Nilsson, H. J.; Tyliszczak, T.; Wilson, R. E.; Werme, L.; Shuh, D. K. *Anal. Bioanal. Chem.* **2005**, *383*, 41−47.
(42) Minasian, S. G.; Keith, J. M.; Batista, E. R.; Boland, K. S.; Bradley, J. A.; Daly, S. R.; Kozimor, S. A.; Lukens, W. W.; Martin, R. L.; Nordlund, D.; Seidler, G. T.; Shuh, D. K.; Sokaras, D.; Tyliszczak, T.; Wagner, G. L.; Weng, T. C.; Yang, P. *J. Am. Chem. Soc.* **2013**, *135*, 1864−1871.

(43) Moore, K. T.; van der Laan, G. *Rev. Mod. Phys.* **2009**, *81*, 235−298.
(44) Kresse, G.; Furthmuller, J. *Comput. Mater. Sci.* **1996**, *6*, 15−50.
(45) Kresse, G.; Furthmuller, J. *Phys. Rev. B* **1996**, *54*, 11169−11186.
(46) Kresse, G.; Joubert, D. *Phys. Rev. B* **1999**, *59*, 1758−1775.
(47) Ceperley, D. M.; Alder, B. J. *Phys. Rev. Lett.* **1980**, *45*, 566−569.
(48) Hohenberg, P.; Kohn, W. *Phys. Rev. B* **1964**, *136*, B864−&.
(49) Blochl, P. E.; Forst, C. J.; Schimpl, J. *Bull. Mater. Sci.* **2003**, *26*, 33−41.
(50) Monkhorst, H. J.; Pack, J. D. *Phys. Rev. B* **1976**, *13*, 5188−5192.

dx.doi.org/10.1021/ic4026359 | *Inorg. Chem.* 2014, 53, 2506−2515